МАТЕРІАЛОЗНАВСТВО

UDC 678.686:620.22-022.53:621.891
DOI https://doi.org/10.32782/3041-2080/2026-6-9

EFFECT OF Y_2O_3 ON THE TRIBOLOGICAL PROPERTIES OF POLYMER-METAL MM «STAHL 1018» COMPOSITE

Arustamian Artem Serhiiovych,
Doctor of Philosophy,
Associate Professor at the Department of Material Science and Applied Mechanics
LIMITED LIABILITY COMPANY "TECHNICAL UNIVERSITY "METINVEST POLYTECHNIC"
ORCID ID: 0000-00022351-8502

Dan Leonid Oleksandrovych,
Candidate of Technical Sciences, Associate Professor,
Associate Professor at the Department of Metallurgy and Metal Processing
State Higher Education Institution «Pryazovskyi State Technical University»
ORCID ID: 0000-0002-1954-4871

This study examines the tribological characteristics and wear mechanisms of the industrial polymer-metal composite MM «Stahl 1018», modified with a fine-dispersed yttrium oxide (Y_2O_3) filler. The research aims to scientifically justify the use of modifiers to enhance the functional properties of metal-polymers used for restoring and protecting friction surfaces of industrial equipment under intense abrasive wear.

The microstructure and morphology were analyzed using scanning electron microscopy. The results revealed a heterogeneous structure consisting of irregular particles of various sizes, ensuring strong mechanical interlocking. Energy-dispersive X-ray spectroscopy identified a complex chemical composition (Fe, Cr, Al, Si, Y, Ba, and S), confirming uniform filler integration. Raman spectroscopy verified the stability of the polymer matrix, identifying epoxy groups and benzene rings responsible for high adhesion to metallic substrates.

Performance was evaluated through standardized ball-on-disk tribological tests under dry friction conditions. It was experimentally demonstrated that adding 20 vol.% yttrium oxide significantly improves resistance to frictional wear. The specific volumetric wear rate was found to be $W = 600.6 \cdot 10^{-6}$ mm^3/Nm, indicating high wear resistance. These findings confirm the technical efficiency of the modified MM «Stahl 1018» for the repair and renovation of components operating under severe service conditions.

Key words: *polymer-metal composite, MM «Stahl 1018», yttrium oxide, tribological properties, wear resistance, SEM, Raman spectroscopy.*

Арустамян Артем, Дан Леонід. Вплив Y_2O_3 на трибологічні властивості полімер-металевого композиту MM «STAHL 1018»

У цій науковій праці представлено результати комплексного експериментального дослідження трибологічних характеристик та механізмів зносу промислового полімер-металевого композиційного матеріалу марки MM «Stahl 1018», модифікованого шляхом введення дрібнодисперсного наповнювача у вигляді оксиду ітрію (Y_2O_3). Актуальність роботи зумовлена необхідністю наукового обґрунтування вибору модифікаторів для покращення функціональних властивостей металополімерів, які широко застосовуються в інженерній практиці для відновлення геометричних параметрів та захисту поверхонь тертя промислових агрегатів.

За допомогою методу сканувальної електронної мікроскопії було проведено детальний аналіз мікроструктури та морфології отриманого композиту. Встановлено, що матеріал має гетерогенну структуру, сформовану з нерегулярних частинок різного розміру, що забезпечує механічне зчеплення в системі. Проведений енергодисперсійний аналіз дозволив ідентифікувати наявність таких хімічних елементів, як Fe, Cr, Al, Si, Y, Ba та S, що свідчить про складний багатокомпонентний склад наповнювача та рівномірність його інтеграції в об'єм полімеру. Застосування методу Раман-спектроскопії дозволило підтвердити стабільність хімічної структури матриці, ідентифікувавши наявність характерних епоксидних груп та бензольних кілець, які відповідають за формування високих адгезійних властивостей матеріалу до металевої основи.

Експлуатаційна оцінка матеріалу проводилася шляхом трибологічних випробувань за стандартизованим методом «куля на диску» в умовах сухого тертя. Експериментально доведено, що модифікація композиту додаванням 20 % за об'ємом оксиду ітрію суттєво підвищує його опір фрикційному зносу. Визначений показник питомого об'ємного зносу на рівні $W = 600{,}6 \cdot 10^{-6}$ мм^3/Нм демонструє високу зносостійкість матеріалу та його здатність протистояти інтенсивному абразивному впливу. Отримані результати підтверджують технічну доцільність та ефективність використання модифікованого складу MM «Stahl 1018» для проведення ремонтних робіт та реновації зношених вузлів і механізмів, що працюють у важких умовах експлуатації.

Ключові слова: *композит, Y_2O_3, MM «Stahl 1018», спектроскопія, трибологія.*

Introduction. The composite Multimetall (MM) «Stahl 1018» was developed in the early 1990s and has been used for repairing bridge pillars, railroad and highway bridges or canal bridges, machinery parts, etc. Thanks to its good forming properties, the composite can be evenly distributed over the surface to be preserved. Even though the material has been on the market for over 30 years it still requires research, and a few of its properties including tribological properties have not been studied yet. There is very little information in the scientific literature about the application and experimental research on the MM «Stahl 1018» composite. Few available publications reporting the results of experimental research [1–5] can be found. For example, the authors in [2] determined the dependence of the proof stress (theoretical yield point) on such factors as height and diameter of the sample. Experimental results for the test specimens showed that the optimal value of the proof stress corresponded to specimens partly fixed in a metal base at a depth of 1 mm. As a result, the maximum compressive strength σ_m=160 N/mm^2 was obtained. However, it should be noted that the method of conducting experiments presented in paper [4] has a limited applicability, and the empirical relationship of the proof stress calculated by the authors was approximate (σ_m=160 N/mm^2), which affects the error in determining the value of the theoretical yield point. A. Vorona [5] carried out calculations of the strength of the metal-polymer layer of MM composite «Stahl 1018» under comprehensive compression using the program «SolidWorks 2014» and models «CosmosWorks 2006 [5]. In turn, S. Kalinichenko [6] presented the results of mechanical strength tests of the material under cyclic impact loading. The results of experiments showed that the material can withstand only small impact loads (up to E=0.5 J). Under volumetric compression, the strength of the composite under dynamic loading increases many times, and the structure can withstand loads on the load-bearing surfaces of heavily loaded machines, especially rollers on the level of 100 – 200 MPa. The author [6] also determined the elastic modulus and Poisson's ratio for MM material «Stahl 1018» by testing specimens in shear and compression. The value of the obtained modulus of elasticity was 13,200 MPa, staying within the limits established in the technical specifications of the material provided by manufacturer [1]. D. Kakareka [7] experimentally investigated how the material's conditional yield strength depends on such factors as the load amplitude and the method of fixing the composite. Experimental results showed that the maximum stress in the dynamic cycle may exceed by even 50 % the maximum stress under static loading without deforming the material. Thus, the MM composite «Stahl 1018» can operate without deforming the surface at an average load of P = 31 kN and load amplitude of 6 kN. The deformation of samples was observed at a load amplitude of 10 kN and an average load of P ≤ 26 kN. It was concluded from the experiments that placing the composite in an enclosed volume can increase its strength under asymmetric loading cycle conditions. This means that in structures operating under high vibratory loads the composite should be used in a closed volume or in a reinforced version. It was also established in further experiments that temperature affects the strength of the polymer. At 100 °C the strength of the composite was found to be 42.12 MPa while at 20 °C it rose much higher at 93.63 MPa. At a temperature between 50-60 °C the strength was 61 MPa. At 20 °C, the material practically did not deform, whereas at 100°C the deformation resulted in the destruction of the sample.

Research methods and techniques. MM composite «Stahl 1018» is composed of polymers, with a chemically treated epoxy resin, and powder-fillers consisting of stainless steel (steel 18-10, EN 10088) and ceramics. The composite was modified by Y_2O_3 powder. Macroscopic and microstructural observations of the MM «Stahl 1018» composite were carried out with a «JEOL JSM-5500 LV» microscope. To identify the matrix material, specimens were tested by the Raman spectroscopy technique.

Raman spectra were recorded on an InVia Raman Spectrometer (Renishaw) containing an air-cooled charge-coupled device (CCD) detector and a Leica microscope (x50 objective). The spectral resolution was set at 4 cm^{-1}. The 785 nm line of a diode laser was used as an excitation source. The laser power at the output was set at 10 mW. The typical exposure time for each Raman measurement was 20 s with five accumulations (series of five spectra, each accumulated 20 s = 100 s). The spectra were identical except for small differences (up to 5 %) in some band intensities.)

Tests of the friction coefficient and wear index were performed based on ISO 20808:2016 [8–17]. A tribometer, model T-21, manufactured at the Institute of Exploitation Technology in Radom [9–14], was used for this purpose. The apparatus is used to test the tribological wear of a material using the ball-and-disk method in rotary motion. It makes it possible to determine the tribological properties of materials cooperating during sliding friction. The testing system consists of a rotating disc and a statically fixed anti-sample in the form

of a sphere loaded with a preset force (F) pressing it against the rotating disc. The device is controlled by a computer program that continuously records the results in the form of a series of data for later processing. Experiments were conducted using a normal load of 5N and a rotation speed of 120 rpm. For the experiments specimens were used made of MM composite material «Stahl 1018» with dimensions of 15×15 mm and height H = 4 mm. The samples were enriched with Y_2O_3 powder. The samples No. 1, 2, 3 and 4 were added 10 vol%, 20 vol%, 30 vol% and 40 vol% of Y_2O_3 powder, respectively.

Results and discussion. The results of the microstructure study of the MM material «Stahl 1018» modified with Y_2O_3 additive are shown in Fig. 1. The composite contains irregular reinforcing particles with a wide bimodal size range, which are distributed in an epoxy resin-based matrix. The irregular shape of the particles indicates that they were previously produced by a milling process. The microstructure of the composite contains a mixture of particles of different chemical composition, as confirmed by the result of the backscattered electron test (Fig. 1 a and c), where they take on a white to dark graphite color.

Figure 2 shows elemental distribution maps of the analyzed composite material containing O, Cr, Fe, Si, C, Y, Al, S and Ba, respectively. Oxygen, carbon and silicon (Fig. 2 a, e) are located mainly within the matrix of the composite material. Chromium and iron (Fig. 2 b, c) are found within the most abundant, relatively large particles in the composite, and are clearly composed of different phases or solutions. This is confirmed by the bands and areas visible on the map associated with changes in iron concentration (Fig. 2 c). Yttrium and oxygen (Fig. 2 f, a) are localized within the small particles that were introduced into the composite material to increase its resistance to abrasive wear. Aluminum (Fig. 2 g) can be seen within elongated and oval particles, with oxygen and silicon additionally identified in the latter type of particles (Fig. 2 a, d). It is interesting to note that the tested commercial material subjected to modification additionally contains particles made of barium and sulfur (Fig. 2 h, i).

The chemical composition analysis shown in the elemental distribution maps (Fig. 2) reveals that the analyzed reinforced composite is a mixture of particles containing: metal alloys from the Fe-Cr system, metal or alloy containing mainly Al, oxides from the Y-O, Al-Si-O systems and sulfide from the Ba-S system.

Fig. 3 shows the representative Raman spectra of the composite MM, measured at different locations on the surface.

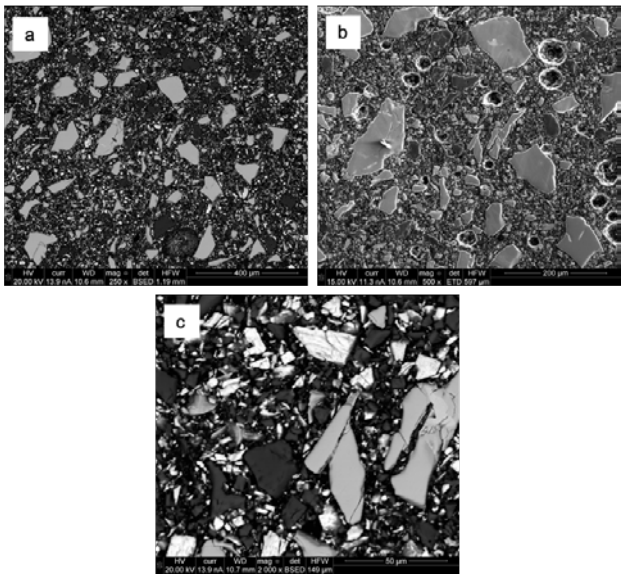

Fig. 1. Microstructure of MM composite «Stahl 1018» modified with Y_2O_3 additives (a, c) – SEM BSED and (b) SEM ETD

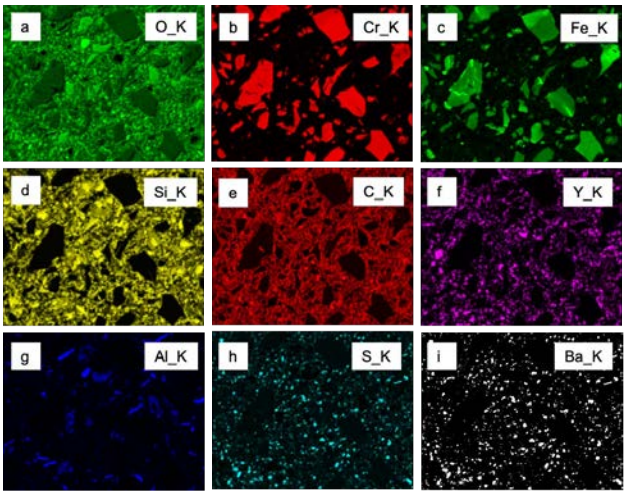

Fig. 2. SEM EDS elemental distribution maps of MM composite material «Stahl 1018» modified with Y_2O_3 additives

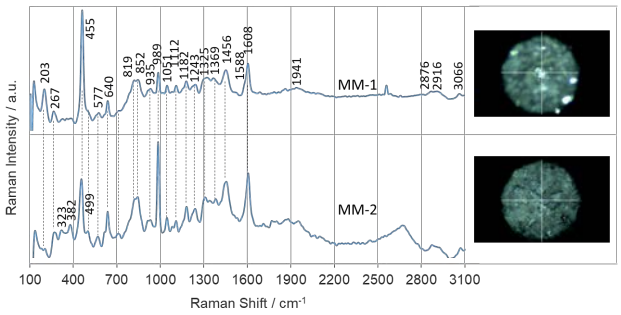

Fig. 3. The representative Raman spectra of the composite MM «Stahl 1018»

In these spectra, several characteristic bands of the epoxide groups can be seen at 935 cm^{-1} (asymmetric

axial stretching at the epoxide ring where the C–C bond increases), at 987, at 1243 cm^{-1} (breathing vibration for the C–O–C of the ether bridge), and at 1182 cm^{-1} (C–O stretching vibration of the secondary alcohol or C–H wagging vibration of epoxy resins) [18–22]. Their intensity is weaker at MM-1 than at MM-2, which is probably due to the process of cleavage of epoxy rings [19; 22]. Also noteworthy is the presence of bands associated with the vibrations of the aromatic benzene ring (φ) at 3066 cm^{-1} (ν(C–H)$_{\varphi}$), at 1608 and 1588 cm^{-1} (ν(C=C)$_{\varphi}$), at 1461 cm^{-1} (ν(C=C) in p-substituted φ), at 1112 cm^{-1} (ν(C–H)$_{\varphi}$ and in-plane epoxy C–H deformation, δ_{ip}(C–H)), at 852 cm^{-1} ($\nu(C_3–C_2)_{skeleton}$), at 819 cm^{-1} (out-of-plane C–H bending, $_{oop}$(C–H)), and at 640 cm^{-1} (δ_{oop}(C–H)) [18; 19; 20; 23; 24]. It should also be noted that the bands at 267, 455, 499, and 1325 cm^{-1} correspond to the vibrations of MgO [25; 26; 27].

The results for sample No. 1 with 10 vol% Y_2O_3 are shown in Figs. 4-5. The test parameters are friction radius – 3 mm; number of cycles – 5,000.

Subsequent experiments for sample No. 1 with 10 vol% Y_2O_3 – are shown in Figs. 6-7. The test parameters are: friction radius – 5 mm; number of cycles – 5,000.

Fig. 4 shows four randomly selected groove profiles obtained by friction with a ball with a 3 mm radius. In another experiment for the same type of sample, the radius of the ball was changed from 3 mm to 5 mm, and the results are shown in Fig. 5. No big difference was observed in the depth and shape of the profiles for these variants, only profile 4 (green) for the case of using a ball radius of 5 mm (Fig. 6) differs by 5 µm, which is within the error limits. The average depth of indentation for specimen 1 after exposure to a ball with a radius of 3 mm, as well as for a ball with a radius of 5 mm, is 26 µm. For these experimental results, the measurement error can be calculated, considering the maximum and minimum peaks of the profile according to formula [28]:

$$\delta = \left[\frac{\Delta x}{x_{\max}}\right]\cdot 100\% = \frac{|x_{\max} - x_{\min}|}{x_{\max}}\cdot 100\% \qquad (1)$$

where:

δ – relative error, %;

$\varnothing x$ – difference between maximum and minimum peak groove, µm;

$x_{\max}$ – maximum groove height, µm;

$x_{\min}$ – minimum groove height, µm

The following was obtained for the analyzed case: x_{max} = – 32 µm, x_{min}= – 28 µm. Substituting the obtained values to equation (1), the relative error was produced:

$$\delta = \frac{|-32-(-28)|}{-32}\cdot 100\% = 12{,}5\%$$

Fig. 4 shows selected images of the surface from the 3D profilometer for sample No. 1 (friction radius – 3 mm). The upper part shows the ball itself with scratches on its surface generated during the experiment. Below are two randomly selected sections of the groove on the sample. The upper picture shows green in the middle, indicating that the depth of the groove reached 30 µm, and the lower picture shows a small cutout of purple color, indicating that the depth at this point is 50 µm. Probably there was a homogeneous element in the composite material at this location, but at the time of the experiment this particle was completely removed from the composite. A similar effect was observed in the experiment with a 5 mm radius bead, except that the maximum groove depth was 35 µm. This difference can be explained by the fact that when using a larger diameter ball, the contact area increases, which reduces the pressure, and a larger diameter ball is less likely to extract various inclusions in the composite material.

The results for sample No. 2 with 20 vol% Y_2O_3 are shown in Figs. 8-10. The test parameters are friction radius – 3 mm; number of cycles – 100,000.

The results for sample No. 2 with 20 vol% Y_2O_3 are shown in Figs. 11 – 13. Test parameters: friction radius – 4 mm; number of cycles – 30,000.

The results for sample No. 2 with 20 vol% Y_2O_3 are shown in Figs. 14 – 16. The test parameters are: friction radius – 5 mm; number of cycles – 5,000.

For sample No. 2 (Fig. 9), the coefficient of friction rapidly increases from 0.1 to 0.45, which is due to the use of a special material (liquid silicone) for samples production, but after 6,000 cycles the silicone film was torn and the ball began to slide on the surface of the composite material. In Fig.s 10, 13 and 16, a similar result is observed as for specimen No. 1, using a ball with a radius of 3 mm. The maximum depth of the groove was 45 µm (Fig. 8), for 4 mm (Fig. 11), and for 5 mm (Fig. 14) – 25 µm. When a ball with a radius of 4 mm was used (Fig. 13), the coefficient of friction ranged from 0.06 to 0.09, and for a ball with a radius of 5 mm (Fig. 15) from 0.075 to 0.085, but these experiments cannot be taken into account because they were conducted before the experiment with a ball with a radius of 4 mm (Fig. 12) during which a rapid growth in the coefficient of friction was observed.

The results for sample No. 3 with 30 vol% Y_2O_3 are shown in Figs. 17 – 19. The test parameters are: friction radius – 3 mm; number of cycles – 5,000.

Experimental results for sample No. 3 with 30 vol% Y_2O_3 are shown in Figs. 20 – 22. The test parameters are: friction radius – 5 mm; number of cycles – 5,000.

The results for sample No. 4 with 40 vol% Y_2O_3 are shown in Figs. 23 – 25. The test parameters are: friction radius – 3 mm; number of cycles – 5,000.

The results for sample No. 4 with 40 vol% Y_2O_3 are shown in Figs. 26 – 28. The test parameters

are: friction radius – 5 mm; number of cycles – 5,000.

For the samples with the 30% and 40% Y_2O_3 addition, sections of the composite surface are shown in Figs. 19, 22, 25 and 28. As in previous experiments, for sample No. 3 and a ball with a radius of 3 mm, the maximum groove depth was 32 μm (Fig. 17), and the coefficient of friction was 0.48 (Fig. 18). For the same sample but using a ball with a radius of 5 mm, the maximum groove depth was 0.32 μm (Fig. 20), but the coefficient of friction decreased from 0.5 at 1000 cycles to 0.48 at 5,000 cycles (Fig. 21). For specimen No. 4, as for specimen No. 2, an experiment was first conducted with a 5 mm radius ball and a similar effect of a rapid growth in the friction coefficient was observed (Fig. 27) from 0.09 to 0.48, but after 1000 cycles the friction coefficient value dropped to 0.45 after reaching 5,000 cycles. Fig. 23 shows that the maximum groove depth is 0.3 μm, for the sample with 30% Y_2O_3, and the friction coefficient dropped from 0.5 at 1000 cycles to 0.42 at 5,000 cycles (Fig. 24).

The software used for the ITE Radom T-21 tribotester also allows for the automatic calculation of the roughness of the tested material. The values of the surface roughness parameters of the samples before the tribological test are listed in Table 1.

Table 1

Surface roughness parameter values of samples

Sample No.*	*Ra**	*Rz**
Sample No. 1	0.007071	0.017547
Sample No. 2	0.004148	0.015857
Sample No. 3	0.008860	0.016815
Sample No. 4	0.004284	0.012042

** Sample No. 1 has a 10% Y_2O_3 addition; Sample No. 2 has a 20% Y_2O_3 addition; Sample No. 3 has a 30% Y_2O_3 addition; Sample No. 4 has a 40% Y_2O_3 addition; Ra – is the arithmetic mean deviation from the mean line [28]; Rz – is the maximum height of roughness according to the measured 10 highest profiles [28]*

The surface roughness of the composite is measured using a pneumatic method, but this method does not provide accurate information. Since the material is polymer-based, its surface is too soft to measure the roughness by traditional methods (optical, pneumatic, interference, etc.). To determine the coefficient of friction, several preliminary tests were carried out, for example, sample No. 2 was tested for 100,000 cycles, but this did not give a clear result, so it was decided to perform 5,000 cycles. The values of the wear index W_v and the average values of the friction coefficient $f_{śr}$ of the samples are listed in Table 2.

Table 2

The value of the wear index W_v and the average value of the friction coefficient $f_{śr}$ of the samples

Sample No.	Parameters	$W_v \times 10^{-6}$ mm^3/Nm	$f_{śr}$
Sample No. 1	R3 5,000 cycles	535.2	-
Sample No. 1	R5 ,5000 cycles	537.3	0.422
Sample No. 2	R3 100,000 cycles	54.3	0.220
Sample No. 2	R4 30,000 cycles	0.24	0.077
Sample No. 2	R5 5,000 cycles	0.85	0.079
Sample No. 3	R3 5,000 cycles	526.8	0.457
Sample No. 3	R5 5,000 cycles	600.6	0.457
Sample No. 4	R3 5,000 cycles	450.7	0.458
Sample No. 4	R5 5,000 cycles	373.9	0.347

Conclusions. Based on the research findings for the "Stahl 1018" MM composite modified with yttrium oxide (Y_2O_3), the following expanded conclusions can be formulated.

1. Scanning electron microscopy (SEM) confirmed that the composite consists of irregular reinforcing particles with a wide bimodal size range distributed within an epoxy resin-based matrix.

2. Elemental mapping revealed a complex mixture of particles, including metal alloys from the Fe-Cr system, aluminum-based alloys, yttrium-oxygen (Y-O) and aluminum-silicon-oxygen (Al-Si-O) oxides, as well as barium-sulfur (Ba-S) sulfides.

3. Raman spectroscopy confirmed the presence of characteristic epoxy groups and benzene rings in the matrix, as well as vibrations corresponding to MgO.

4. The addition of 20 vol% yttrium oxide has a positive effect on friction wear resistance, although its overall impact on improving wear resistance is considered minor.

5. For samples with 10 vol% Y_2O_3, the friction coefficient was approximately 0.51. In samples with 20 vol% Y_2O_3, the coefficient increased from 0.1 to 0.45 after the initial silicone film was torn during testing.

6. The average indentation depth for the samples was approximately 26 μm. Increasing the radius of the friction ball (from 3 mm to 5 mm) reduces the likelihood of extracting inclusions from the composite due to increased contact area and reduced pressure.

7. The material exhibits high wear resistance, with a maximum determined volumetric wear of W = 600.6 $\cdot 10^{-6}$ mm^3/Nm.

8. Under volumetric compression, the material can withstand significant loads on load-bearing surfaces, ranging from 100 to 200 MPa.

9. Strength is highly dependent on temperature; the compressive strength drops from 93.63 MPa at 20

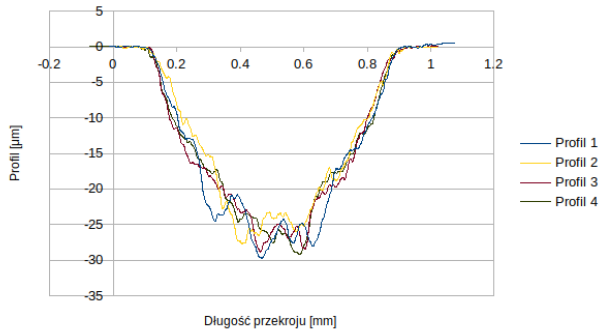

Fig. 4. Measured groove profiles at four points for sample No. 1 with 10 vol% Y_2O_3 , Profile height/Distance – 30 µm/94 m

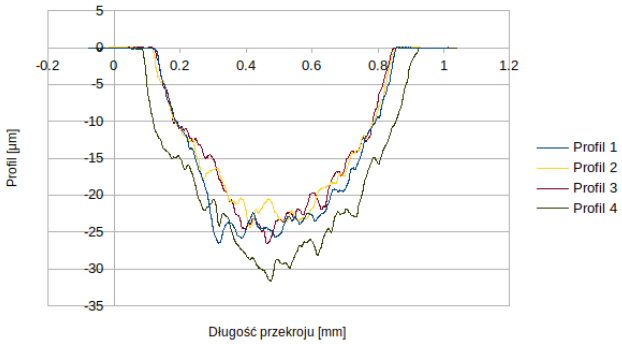

Fig. 6. Measured groove profiles at four locations for sample No. 1 with 10 vol% Y_2O_3

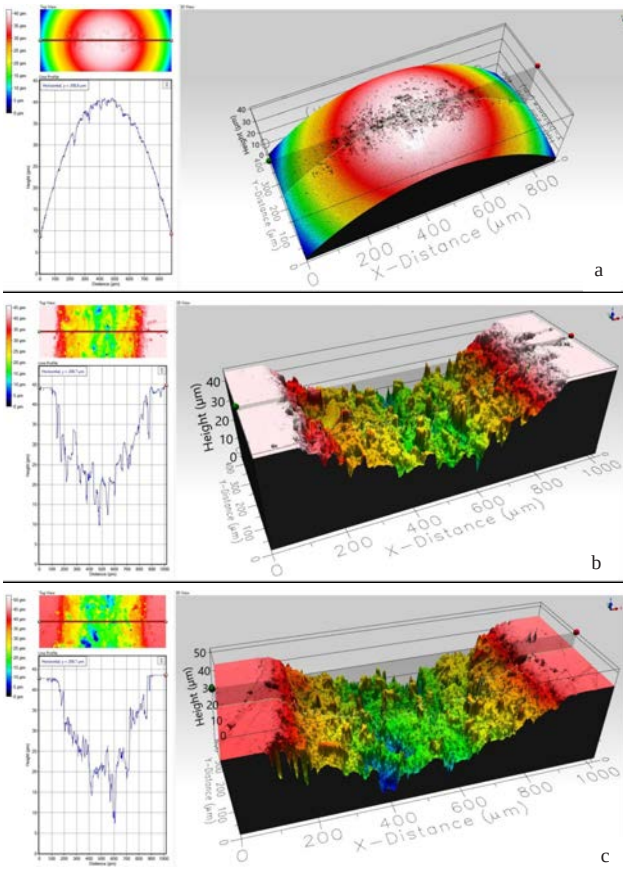

Fig. 5. Selected images of the surface from 3D profilometer for sample No. 1 (friction radius – 3 mm, number of cycles – 5,000). (a) for the anti-sample ball, (b, c) for the surface of the sample

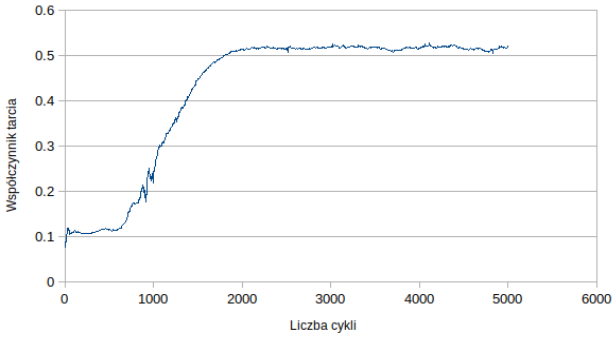

Fig. 7. Change in friction coefficient as a function of the number of cycles for sample No. 1 with 10 vol% Y_2O_3. Friction coefficient/ No. of cycles – 0.51/5000

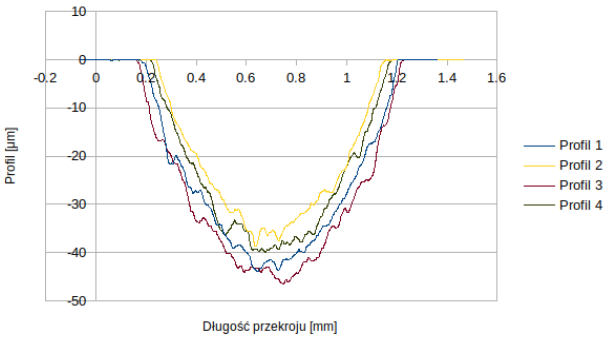

Fig. 8. Measured groove profiles at four locations for sample No. 2 with 20 vol% Y_2O_3

°C to 42.12 MPa at 100 °C. At 100 °C, the material undergoes deformation leading to sample destruction.

10. The composite is highly recommended for the repair and restoration of worn industrial equipment operating under conditions of intense friction.

11.For structures subjected to high vibratory or asymmetric loads, it is advised to use the composite in an enclosed volume or a reinforced version to increase its strength.

12. While current tests were conducted at 20 °C, further research is suggested for temperatures between 40 °C and 80 °C to better understand its performance in real-world operating environments.

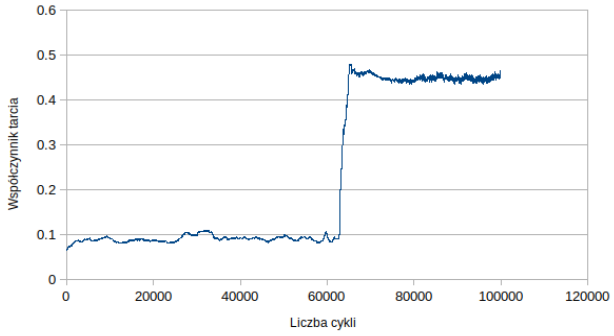

Fig. 9. Change in friction coefficient as a function of the number of cycles for sample No. 2 with 20 vol% Y_2O_3

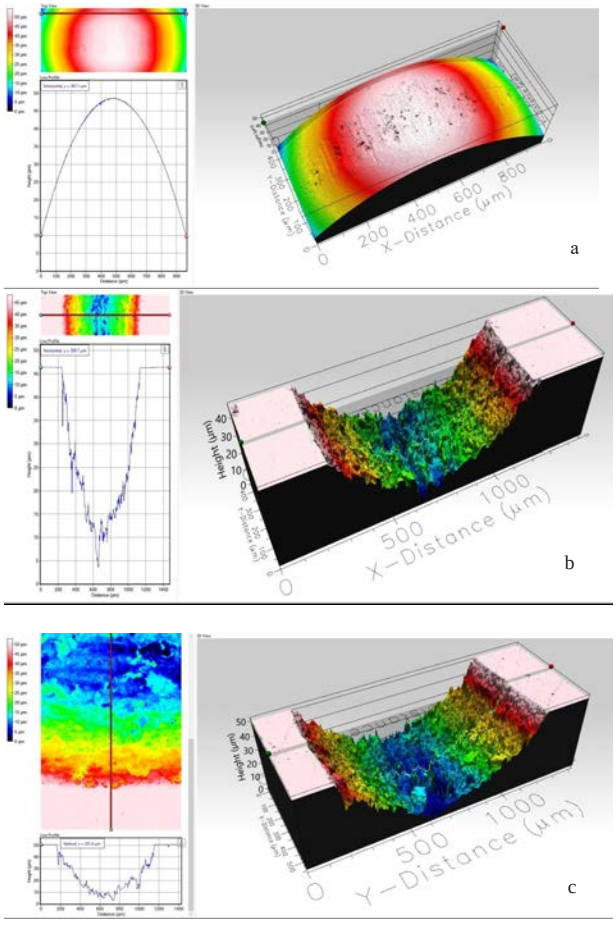

Fig. 10. Selected images of the surface from the 3D profilometer for sample No. 2 (friction radius – 3 mm, number of cycles – 100,000). (a) For the anti-sample ball, (b, c) for the sample surface

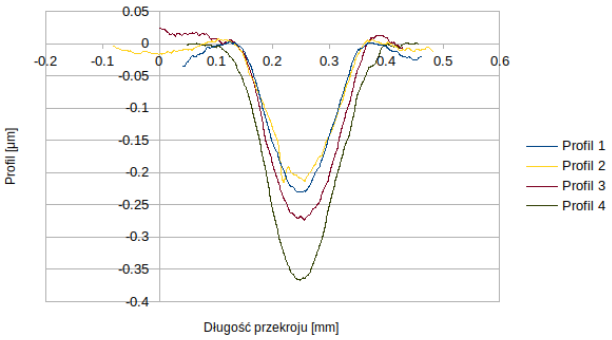

Fig. 11. Measured groove profiles at four locations for sample No. 2 with 20 vol% Y_2O_3

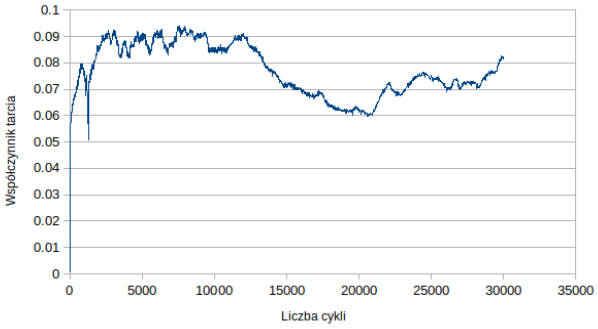

Fig. 12. Change in friction coefficient as a function of the number of cycles for sample No. 2 with 20 vol% Y_2O_3.

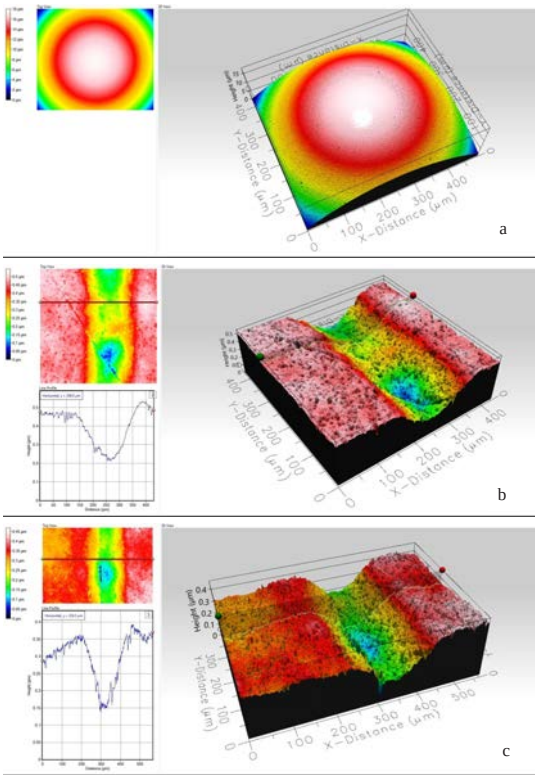

Fig. 13. Selected images of the surface from the 3D profilometer for sample No. 2 (friction radius – 4 mm, number of cycles – 30,000). (a) for the anti-sample ball, (b, c) for the sample surface

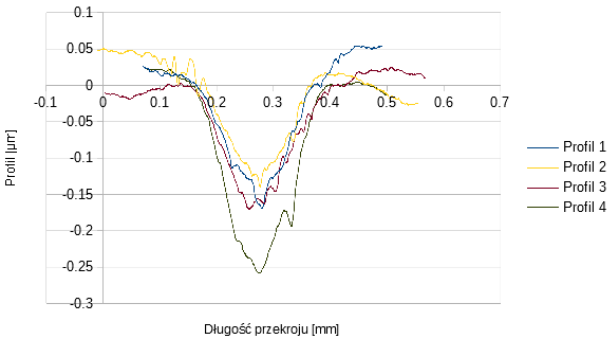

Fig. 14. Measured groove profiles at four locations for sample No. 2 with 20 vol% Y_2O_3

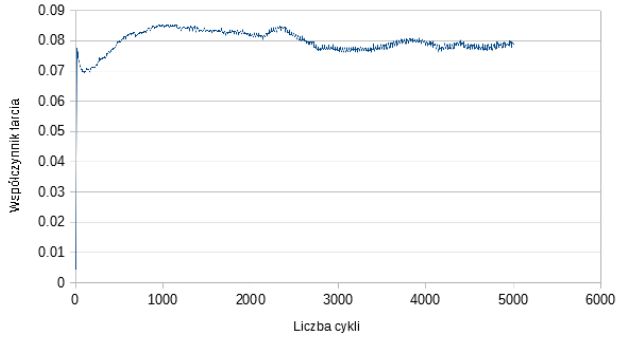

Fig. 15. Change in friction coefficient as a function of the number of cycles for sample No. 2 with 20 vol% Y_2O_3

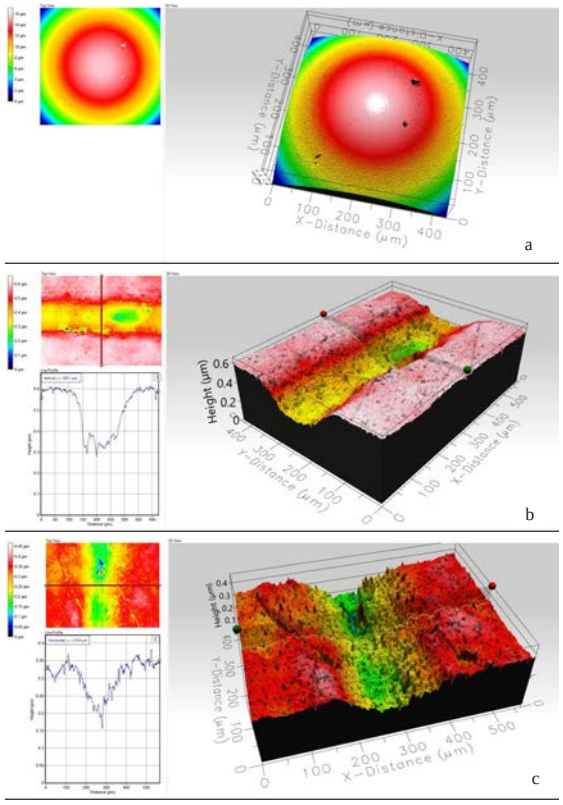

Fig. 16. Selected images of the surface from the 3D profilometer for sample No. 2 (friction radius – 5 mm, number of cycles – 5000). (a) For the anti-sample ball, (b, c) for the sample surface

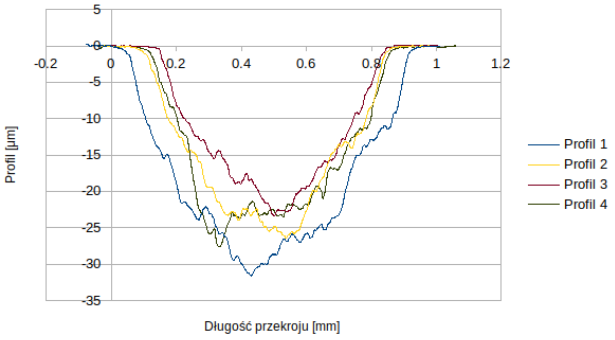

Fig. 17. Measured groove profiles at four locations for sample No. 3 with 30 vol% Y_2O_3

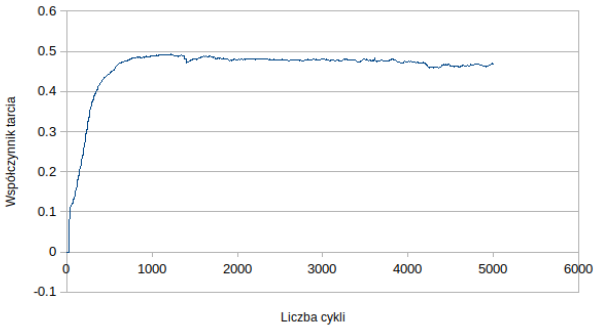

Fig. 18. Change in friction coefficient as a function of the number of cycles for sample No. 3 with 30 vol% Y_2O_3

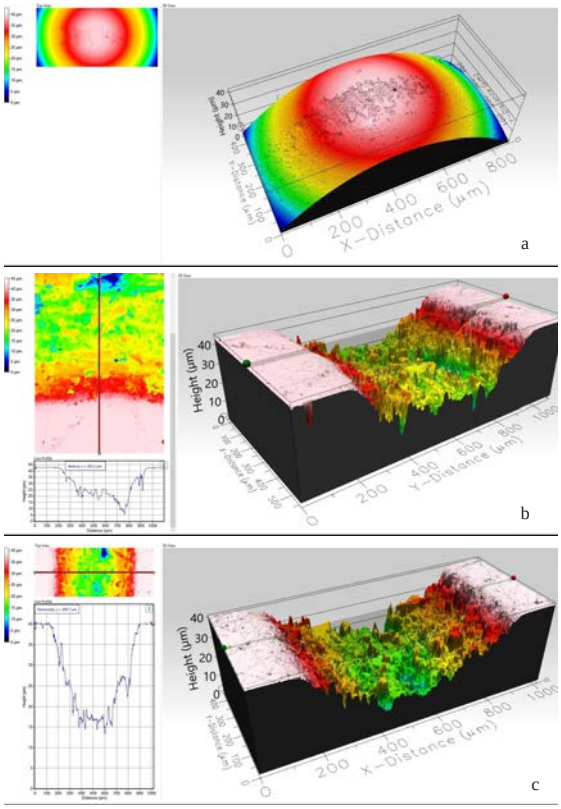

Fig. 19. Selected images of the surface from the 3D profilometer for sample No. 3 (friction radius – 3 mm, number of cycles – 5,000). (a) for the anti-sample ball, (b, c) for the sample surface

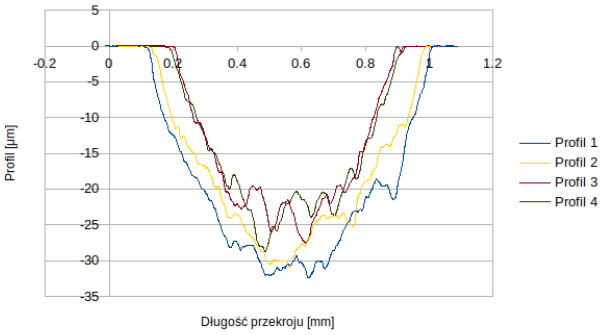

Fig. 20. Groove profiles measured at four locations for sample No. 3 with 30 vol% Y_2O_3

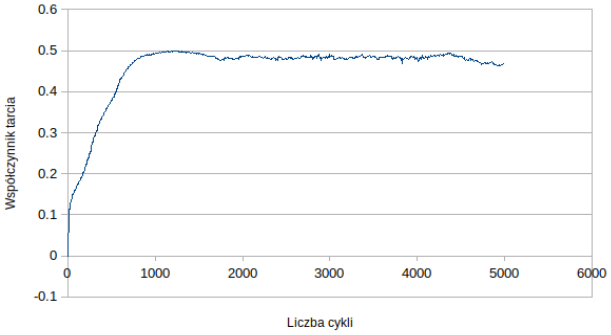

Fig. 21. Change in friction coefficient as a function of the number of cycles for sample No. 3 with 30 vol% Y_2O_3

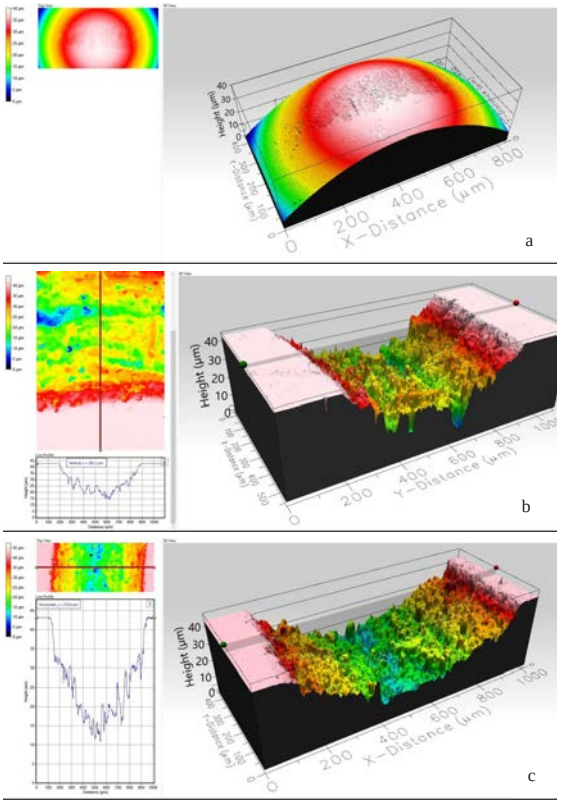

Fig. 22. Selected images of the surface from the 3D profilometer for sample No. 3 (friction radius – 5 mm, number of cycles – 5,000). (a) for the anti-sample ball, (b, c) for the sample surface

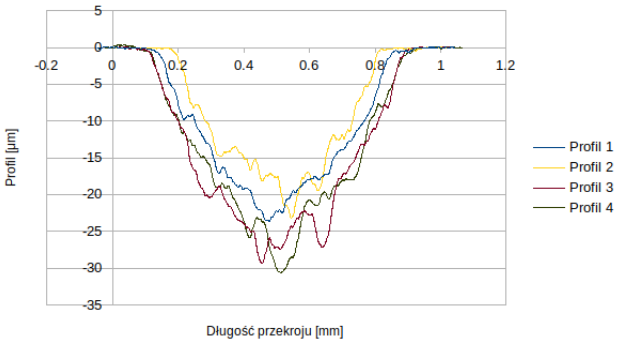

Fig. 23. Measured groove profiles at four locations for sample No. 4 with 40 vol% Y_2O_3

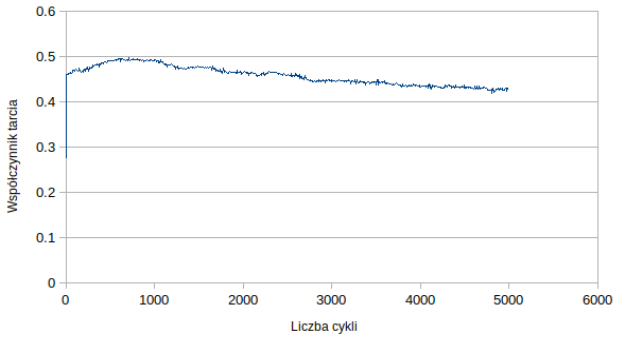

Fig. 24. Change in friction coefficient as a function of the number of cycles for sample No. 4 with 40 vol% Y_2O_3

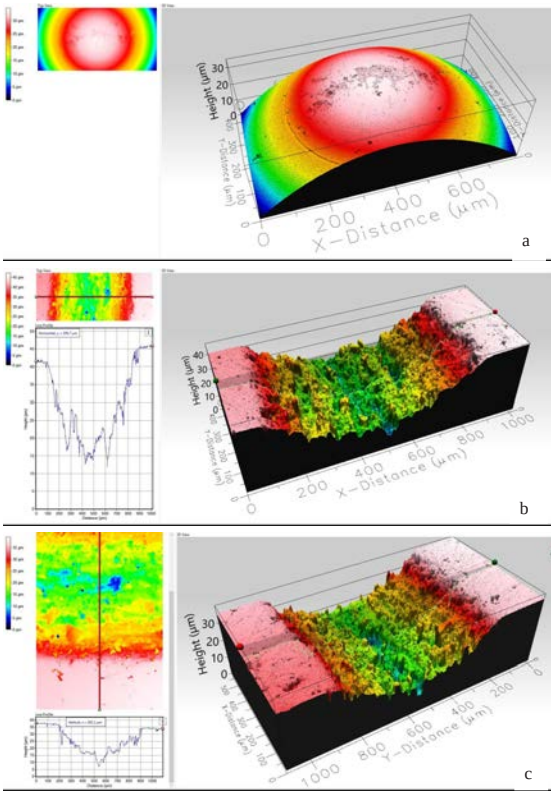

Fig. 25. Selected images of the surface from the 3D profilometer for sample No. 4 (friction radius – 3 mm, number of cycles – 5,000). (a) For the anti-sample ball, (b, c) for the sample surface

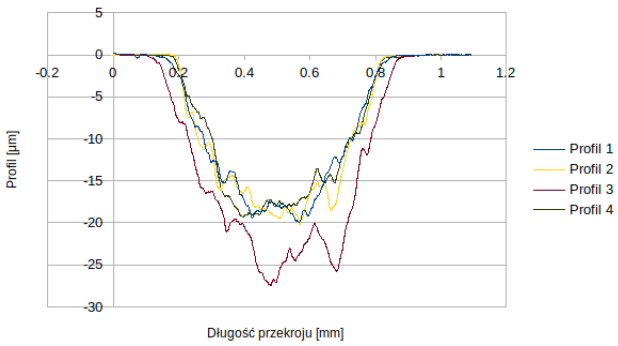

Fig. 26. Measured groove profiles at four locations for sample No. 4 with 40 vol% Y_2O_3

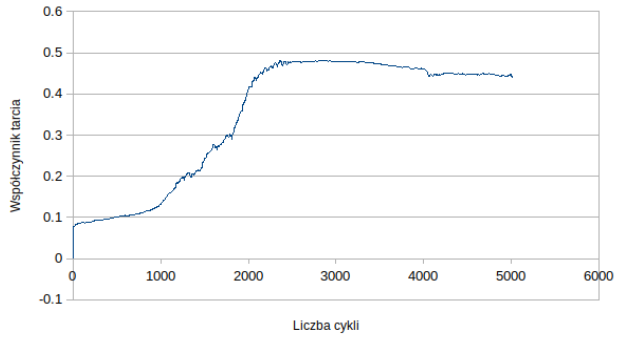

Fig. 27. Change in friction coefficient as a function of the number of cycles for sample No. 4 with 40 vol% Y_2O_3

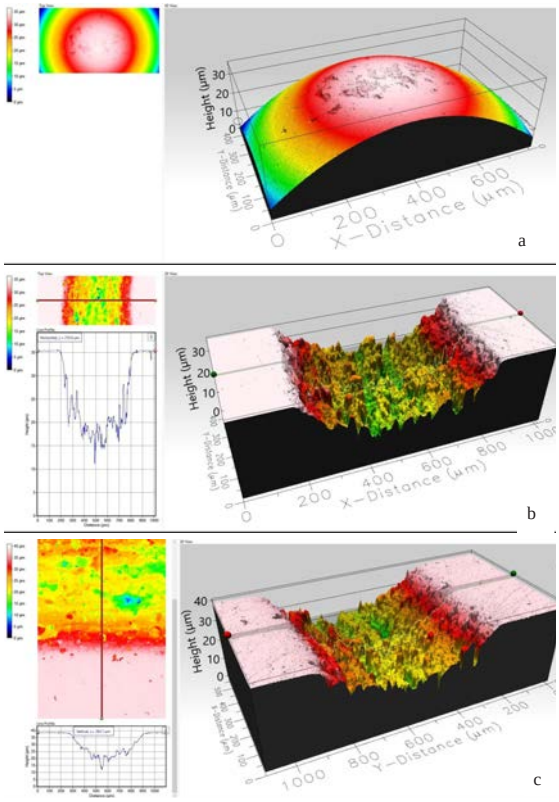

Fig. 28. Selected images of the surface from the 3D profilometer for specimen No. 4 (friction radius – 5 mm, number of cycles – 5,000). (a) For the anti-sample ball, (b, c) for the sample surface

BIBLIOGRAPHY:

1. Ischenko A. A. Technological bases of restoration of the industrial equipment by modern polymeric materials. *Reporter of the Priazovskyi State Technical University. Section: Technical sciences*. 2012. Issue 24. P. 27–39.

2. Banat D., Mania R. J. Comparison of failure criteria application for FML column buckling strength analysis. *Composite Structures*. 2016. Vol. 140. P. 806–815.

3. Timoschenko A. V. Research of the mechanical properties of composite materials under dynamic loading : Master's thesis / Priazovskyi State Technical University. Mariupol, 2010.

4. Donev K. V. Investigation of the properties of metalpolymer materials and the development of technology of repair roughing stand : Master's thesis / Priazovskyi State Technical University. Mariupol, 2007.

5. Vorona A. S. Theoretical and experimental research of the mechanical properties of polymer repair materials for different purposes : Master's thesis / Priazovskyi State Technical University. Mariupol, 2009.

6. Kalinichenko S. A. Research of the dynamic properties of metal-polymer materials : Master's thesis / Priazovskyi State Technical University. Mariupol, 2003.

7. Kakareka D. L. Research of the mechanical properties of composite materials under dynamic loading : Master's work / Priazovskyi State Technical University. Mariupol, 2013.

8. Bamford C. H., Tipper C. F. H. Comprehensive chemical kinetics: Degradation of polymers. Elsevier, 1975. 535 p.

9. A comparative study of epoxy and polyurethane based coatings containing polyaniline-DBSA pigments for corrosion protection on mild steel / F. B. Diniz et al. *Progress in Organic Coatings*. 2013. Vol. 76, no. 5. P. 912–916.

10. Raman and Near-Infrared Studies of an Epoxy Resin / K. E. Chike et al. *Applied Spectroscopy*. 1993. Vol. 47, no. 10. P. 1631–1635.

11. Contu F., Fenzy L., Taylor S. R. An FT-IR investigation of epoxy coatings as a function of electrolyte composition. *Progress in Organic Coatings*. 2012. Vol. 75, no. 1-2. P. 92–96.

12. FM and XRD Characterization of Silver Nanoparticles Films Deposited on the Surface of DGEBA Epoxy Resin by Ion Sputtering / J. E. de Andrade et al. *Polímeros*. 2013. Vol. 23, no. 1. P. 19–23.

13. A study by Raman, near-infrared and dynamic-mechanical spectroscopies on the curing behaviour, molecular structure and viscoelastic properties of epoxy/anhydride networks / P. Musto et al. *Polymer*. 2007. Vol. 48, no. 13. P. 3703–3716.

14. Effect of UV radiation on some semi-interpenetrating polymer networks based on polyurethane and epoxy resin / D. Rosu et al. *Polymer Degradation and Stability*. 2012. Vol. 97, no. 8. P. 1261–1269.

15. The kinetics of the cure of an advanced epoxy resin by Fourier transform Raman and near-IR spectroscopy / C. J. DeBakker et al. *Spectrochimica Acta Part A: Molecular and Biomolecular Spectroscopy*. 1993. Vol. 49, no. 5-6. P. 739–752.

16. Synthesis, structure and thermal properties of montmorillonite/ionic liquid ionogels / A. V. Noskov et al. *RSC Advances*. 2020. Vol. 10, no. 58. P. 34885–34894.

17. A Novel Method to Improve the Anticancer Activity of Natural-Based Hydroxyapatite against the Liver Cancer Cell Line Hep G2 Using Mesoporous Magnesia as a Micro-Carrier / N. S. Awwad et al. *Molecules*. 2017. Vol. 22, no. 11. Art. no. 1947.

18. In vitro evaluation of the toxic effects of MgO nanostructure in Hela cell line / M. W. Akram et al. *Scientific Reports*. 2018. Vol. 8. Art. no. 4576.

19. Barbero E. J. Finite element analysis of composite materials using ANSYS. 2nd ed. CRC Press, 2014. 544 p.

20. Barcikowski M. Wpływ materiałów i struktury laminatów poliestrowo-szklanych na ich odporność na udar balistyczny : rozprawa doktorska / Zachodniopomorski Uniwersytet Technologiczny w Szczecinie. Szczecin, 2012.

21. Mechanical fatigue degradation of ceramics versus resin composites for dental restorations / R. Belli et al. *Dental Materials*. 2014. Vol. 30, no. 4. P. 424–432.

22. Bełzowski A. Metoda oceny stopnia uszkodzenia kompozytów polimerowych. *Kompozyty (Composites)*. 2002. Vol. 2, no. 4. P. 253–258.

23. Benmokrane B., Zhang B., Chennouf A. Tensile properties and pullout behaviour of AFRP and CFRP rods for grouted anchor applications. *Construction and Building Materials*. 2000. Vol. 14, no. 3. P. 157–170.

24. Durand L. P. Composite materials research progress. Nova Science Publishers, 2008. 317 p.

25. Modeling of MnS precipitation during the crystallization of grain oriented silicon steel / D. Kalisz et al. *Metalurgija*. 2015. Vol. 54, no. 1. P. 139–142.

26. Fejdyś M., Łandwijt M. Włókna techniczne wzmacniające materiały kompozytowe. *Techniczne Wyroby Włókiennicze*. 2010. Nr. 1-2. P. 12–22.

27. Gadomski J. Badanie degradacji kompozytu węglowego za pomocą metody tomografii rezystancyjnej : rozprawa doktorska / Oficyna Wydawnicza Politechniki Warszawskiej. Warszawa, 2013.

28. Investigation of in situ and ex situ catalytic pyrolysis of miscanthus × giganteus using a PyGC–MS microsystem and comparison with a bench-scale spouted-bed reactor / D. P. Gamliel et al. *Bioresource Technology*. 2015. Vol. 191. P. 187–196.

REFERENCES:

1. Ischenko, A. A. (2012). *Technological bases of restoration of the industrial equipment by modern polymeric materials*. PSTU (Mariupol), 27–39.

2. Banat, D., & Mania, R. J. (2016). Comparison of failure criteria application for FML column buckling strength analysis. *Composite Structures*.

3. Timoschenko, A. V. (2010). *Research of the mechanical properties of composite materials under dynamic loading* [Master's thesis, PSTU]. Mariupol, Ukraine.

4. Donev, K. V. (2007). *Investigation of the properties of metalpolymer materials and the development of technology of repair roughing stand* [Master's thesis, PSTU]. Mariupol, Ukraine.

5. Vorona, A. S. (2009). *Theoretical and experimental research of the mechanical properties of polymer repair materials for different purposes* [Master's thesis, PSTU]. Mariupol, Ukraine.

6. Kalinichenko, S. A. (2003). *Research of the dynamic properties of metal-polymer materials* [Master's thesis, PSTU]. Mariupol, Ukraine.

7. Kakareka, D. L. (2013). *Research of the mechanical properties of composite materials under dynamic loading* [Master's work, PSTU]. Mariupol, Ukraine.

8. Bamford, C. H., & Tipper, C. F. H. (1975). *Comprehensive chemical kinetics: Degradation of polymers*. Elsevier.

9. Diniz, F. B., De Andradea, G. F., Martins, C. R., & De Azevedo, W. M. (2013). A comparative study of epoxy and polyurethane based coatings containing polyaniline-DBSA pigments for corrosion protection on mild steel. *Progress in Organic Coatings, 76*(5), 912–916.

10. Chike, K. E., Myrick, M. L., Lyon, R. E., & Angel, S. M. (1993). Raman and Near-Infrared Studies of an Epoxy Resin. *Applied Spectroscopy, 47*(10), 1631–1635.

11. Contu, F., Fenzy, L., & Taylor, S. R. (2012). An FT-IR investigation of epoxy coatings as a function of electrolyte composition. *Progress in Organic Coatings, 75*(1-2), 92–96.

12. de Andrade, J. E., Machado, R., Macêdo, M. A., & Cunha, F. G. C. (2013). FM and XRD Characterization of Silver Nanoparticles Films Deposited on the Surface of DGEBA Epoxy Resin by Ion Sputtering. *Polímeros, 23*(1), 19–23.

13. Musto, P., Abbate, M., Ragosta, G., & Scarinzi, G. (2007). A study by Raman, near-infrared and dynamic-mechanical spectroscopies on the curing behaviour, molecular structure and viscoelastic properties of epoxy/anhydride networks. *Polymer, 48*(13), 3703–3716.

14. Rosu, D., Rosu, L., Mustata, F., & Varganici, C.-D. (2012). Effect of UV radiation on some semi-interpenetrating polymer networks based on polyurethane and epoxy resin. *Polymer Degradation and Stability, 97*(8), 1261–1269.

15. DeBakker, C. J., George, G. A., St John, N. A., & Fredericks, P. M. (1993). The kinetics of the cure of an advanced epoxy resin by Fourier transform Raman and near-IR spectroscopy. *Spectrochimica Acta Part A: Molecular and Biomolecular Spectroscopy, 49*(5-6), 739–752.

16. Noskov, A. V., Alekseeva, O. V., Shibaeva, V. D., & Agafonov, A. V. (2020). Synthesis, structure and thermal properties of montmorillonite/ionic liquid ionogels. *RSC Advances, 10*(58), 34885–34894.

17. Awwad, N. S., Alshahrani, A. M., Saleh, K. A., & Hamdy, M. S. (2017). A Novel Method to Improve the Anticancer Activity of Natural-Based Hydroxyapatite against the Liver Cancer Cell Line Hep G2 Using Mesoporous Magnesia as a Micro-Carrier. *Molecules, 22*(11), 1947.

18. Akram, M. W., Fakhar-e-Alam, M., Atif, M., Butt, A. R., Asghar, A., Jamil, Y., Alimgeer, K. S., & Wang, Z. M. (2018). In vitro evaluation of the toxic effects of MgO nanostructure in Hela cell line. *Scientific Reports, 8*, 4576.

19. Barbero, E. J. (2014). *Finite element analysis of composite materials using ANSYS*. CRC Press.

20. Barcikowski, M. (2012). *Wpływ materiałów i struktury laminatów poliestrowo-szklanych na ich odporność na udar balistyczny* [Doctoral dissertation, Zachodniopomorski Uniwersytet Technologiczny w Szczecinie].

21. Belli, R., Geinzer, E., Muschweck, A., Petschelt, A., & Lohbauer, U. (2014). Mechanical fatigue degradation of ceramics versus resin composites for dental restorations. *Dental Materials, 30*(4), 424–432.

22. Bełzowski, A. (2002). Metoda oceny stopnia uszkodzenia kompozytów polimerowych. *Kompozyty (Composites), 2*(4), 253–258.

23. Benmokrane, B., Zhang, B., & Chennouf, A. (2000). Tensile properties and pullout behaviour of AFRP and CFRP rods for grouted anchor applications. *Construction and Building Materials, 14*(3), 157–170.

24. Durand, L. P. (2008). *Composite materials research progress*. Nova Science Publishers.

25. Kalisz, D., Żak, P. L., Lelito, J., Szucki, M., Suchy, J. S., & Gracz, B. (2015). Modeling of MnS precipitation during the crystallization of grain oriented silicon steel. *Metalurgija, 54*(1), 139–142.

26. Fejdyś, M., & Łandwijt, M. (2010). Włókna techniczne wzmacniające materiały kompozytowe. *Techniczne Wyroby Włókiennicze*, 12–22.

27. Gadomski, J. (2013). *Badanie degradacji kompozytu węglowego za pomocą metody tomografii rezystancyjnej* [Doctoral dissertation, Oficyna Wydawnicza Politechniki Warszawskiej].

28. Gamliel, D. P., Du, S., Bollas, G. M., & Valla, J. A. (2015). Investigation of in situ and ex situ catalytic pyrolysis of miscanthus × giganteus using a PyGC–MS microsystem and comparison with a bench-scale spouted-bed reactor. *Bioresource Technology, 191*, 187–196.

Дата першого надходження статті до видання: 26.11.2025
Дата прийняття статті до друку після рецензування: 16.12.2025
Дата публікації (оприлюднення) статті: 16.03.2026